Dependence of count rate on magnetic field in superconducting thin-film TaN single-photon detectors

Engel, Andreas ; Schilling, Andreas ; Il'in, Konstantin ; Siegel, Michael

DOI: https://doi.org/10.1103/PhysRevB.86.140506

Magnetic-field dependence of count rates in superconducting thin-film TaN single-photon detectors

Andreas Engel* and Andreas Schilling

Physics Institute of the University of Zurich,

Winterthurerstr. 190, 8057 Zurich, Switzerland

Konstantin Il'in and Michael Siegel

Institute of Micro- and Nano-Electronic Systems,

Karlsruhe Institute of Technology, Hertzstr. 16, 76187 Karlsruhe, Germany

(Dated: October 2, 2012)

Abstract

We have studied the magnetic-field dependence of both dark-count rates and photon-count rates in a superconducting nanowire single-photon detector made of TaN in external magnetic fields $|\mu_0 H| < 10$ mT perpendicular to the plane of the underlying meander structure and at $T = 4$ K. The dark-count rates show a characteristic field-dependence, which is asymmetric with respect to magnetic field direction. The field- and the current dependence of the dark counts can be quantitatively well explained if one assumes that the critical current is reduced to $\approx 50\%$ at the 180° meander turns when compared to a straight strip, and the observed asymmetry can be modeled assuming that the turnarounds are not all strictly equal. Surprisingly, the photon count rates do not show any significant field dependence, which seems to be at odds with existing detection models invoking vortex crossings.

PACS numbers: 74.40.+k, 74.78.Na

Magnetic vortices in meso- and microscopic superconducting structures display a rich variety of phenomena. Since in many applications such structures are composed of arrays of superconducting strips, the strip geometry is of particular interest. It has been realized theoretically[1,2] and experimentally[3] that narrow superconducting strips remain in the Meissner state up to magnetic fields significantly exceeding the lower critical field H_{c1} of the bulk material. However, if a transport current is applied, vortices (or anti-vortices) may be activated over the energy barrier at the strip edges that subsequently traverse the strip under the influence of the Lorentz-force, thereby destroying the dissipation-free superconducting state[4]. Currently there is a debate[5–9] over the fluctuation modes dominating in thin superconducting strips that are too wide to be considered one-dimensional, *i.e.*, with width $w \gg \xi$, the superconducting coherence length, but narrow enough so that edge-effects are significant, *i.e.* $w \ll \Lambda$, where $\Lambda = 2\lambda^2/d$ is the effective penetration depth, λ is the magnetic penetration depth in thick films and $d \ll \lambda$ is the film thickness. This situation is typical for superconducting nanowire single-photon detectors[10] (SNSPD), where a large bias current is applied which is of the order of the experimental critical current. Vortices crossing the superconducting strip have been considered as the main cause for dark-count events[6,11] in SNSPD. Vortices have also been made responsible to explain the detection of low-energy photons for which the photon energy alone is insufficient to trigger a detection event[8,12]. Both events, dark counts as well as vortex-assisted photon counts, should have a distinct magnetic-field dependence[8].

The detection elements of SNSPD are not simply straight strips, however. In order to increase the effective detection area and the coupling to the electro-magnetic wave of the photons, the active area typically consists of a meander with separations between adjacent strips roughly equal to the strip width. This design implies 180° turnarounds at the strip ends for the superconducting bias-current. Whereas the current-density along the straight portions of the meander is highly uniform, due to the fact that $w \ll \Lambda$, the current density is inhomogeneous in the vicinity of the turnarounds[13]. The local current density at the inner radius of the turnaround exceeds the uniform current density of the straight parts and it is reduced at the outer radius. This leads to an effectively reduced critical current for a meander structure, because superconductivity is destroyed when the energy barrier vanishes at the inner radius. For the geometry considered here, the corresponding current density is always lower than the depairing current-density[6]. The level of reduction of the critical

current depends on the detailed geometry of the turn[14,15] and can be minimized to achieve higher critical currents for meander structures[16]. In the case of a single turn or several turns in the same direction, the application of a small magnetic field of the right orientation should lead to an increase of the critical current[17].

In this Rapid Communication we report on systematic measurements of the magnetic field-dependence of dark counts as well as photon counts in SNSPD. The device studied in detail is made from a $d = 4.9$ nm thick TaN film deposited by DC reactive magnetron sputtering on a R-plane cut sapphire substrate[18]. Using electron-beam lithography the film was patterned into a meander with 21 strips of width $w = 110$ nm, strip separation $\Delta = 80$ nm and covering an area of 3.4×3.9 μm^2. Such TaN-SNSPD have been demonstrated to be single-photon detectors comparing favorably well with NbN-SNSPD[19]. After fabrication the device had a sharp superconducting transition[8,11,20–22,24] at $T_c = 8.84$ K. Count-rate measurements were done in a He-3 cryostat with free-space optical access. The light from a continuous light-source was passed through a monochromator and directed onto the detector through a series of quartz windows and apertures with decreasing diameter to reduce the amount of blackbody background radiation. For the measurements of the intrinsic dark counts caused by fluctuations in the superconducting meander, the optical windows were replaced by blanks and an Al cap was placed over the detector in good thermal contact to the sample holder, thereby creating an isothermal cavity around the detector.

The bias current was supplied by a *Keithley 2400* programmable source-measure unit. To ensure a stable DC current through the detector, a series of HF- and low-pass filters was used. The detector signal was fed into a cryogenic amplifier at the 4K-stage and then further amplified at room-temperature before fed into a threshold counter. Further details of the used set-up are given elsewhere[19]. A bipolar magnetic field up to about 10 mT was applied using a conventional electro-magnet placed as close as possible to the device outside the cryostat and opposite to the optical access window. In this way the magnetic field was oriented perpendicular to the meander plane. The magnetic field was measured using a calibrated cryogenic hall-sensor that was placed in close proximity to the detector inside the cryostat. We verified field gradients to be negligible over the small detector area due to a minimum distance of the magnet to the detector of about 6 cm[25]. All measurements presented have been done at $T = 4$ K.

In Fig. 1 the dark-count rate R_{DC} in zero magnetic field is plotted on a logarithmic scale

vs. the applied bias current I_b. It shows the typical near-exponential increase for increasing bias currents. The solid line is a fit of Eq. (51) from Ref. 6 to our data with an attempt rate and the vortex energy scale ν as free parameters (solid line in Fig. 1). We obtain an almost identical current-dependence upon reversing the current direction, but shifted along the I_b-axis by about 0.4 μA, which is probably caused by an unaccounted current offset (not shown in Fig. 1). From the fitted parameter $\nu = \varepsilon_0/(k_B T) = 51.5 \pm 1.5$, $\varepsilon_0 = \Phi_0^2 \mu^2/(2\pi\mu_0\Lambda)$ (Refs. 6,8), we can derive the effective penetration depth at $T = 4$ K, $\Lambda = 165 \pm 5$ μm, which compares very well with ~ 120 μm, the zero-T value expected from our conductivity measurements, where $\Phi_0 = 2.068 \times 10^{-15}$ Wb is the magnetic-flux quantum, $\mu = 0.930$ a correction for currents close to the depairing current, $\mu_0 = 4\pi \times 10^{-7}$ Vs/Am is the vacuum permeability and $k_B = 1.38 \times 10^{-23}$ J/K is Boltzmann's constant.

For the description of the magnetic-field dependence of the dark-count rate we can phenomenologically approximate the current-dependence as

$$R_{\mathrm{DC}} \approx R_0 \exp\left(\frac{I_b}{\tilde{I}}\right), \tag{1}$$

with R_0 being a proportionality factor, $\tilde{I} \propto I_c$ is a current scale and I_c is the experimental critical current. The dashed line in Fig. 1 as a resulting fit of our data to Eq. (1) shows that for the current-range of interest this is a satisfactory description of the current-dependence of R_{DC}. Using Eq. (1) has the advantage over Eq. (51) of Ref. 6 that the underlying physical model, which we will use to describe the field-dependence, becomes more transparent. In the following we will assume that the experimental critical current I_c is equivalent to the current for which the barrier for vortex entry vanishes at a certain point along an edge of our structure. The experimentally measured $I_c \approx 17$ μA is indicated in Fig. 1.

In Fig. 2 we are plotting the measured R_{DC} as a function of the applied magnetic field H for various bias currents. The upper panel shows the dark-count rates for a certain current direction (in our convention $I_b < 0$) and the lower panel for the reversed current direction ($I_b > 0$), both for positive and negative magnetic-field values. The dark-count rate is clearly magnetic-field dependent with a certain unexpected asymmetry with respect to the field direction. For $I_b > 0$ ($I_b < 0$) the minimum in R_{DC} seems to be shifted to slightly negative (positive) fields. However, reversing both the current and magnetic field direction leaves the asymmetry unchanged as demonstrated for the data measured with $I_b = +16.5$ μA plotted in the upper panel (open symbols), but with a reversed (upper) field-axis from +10

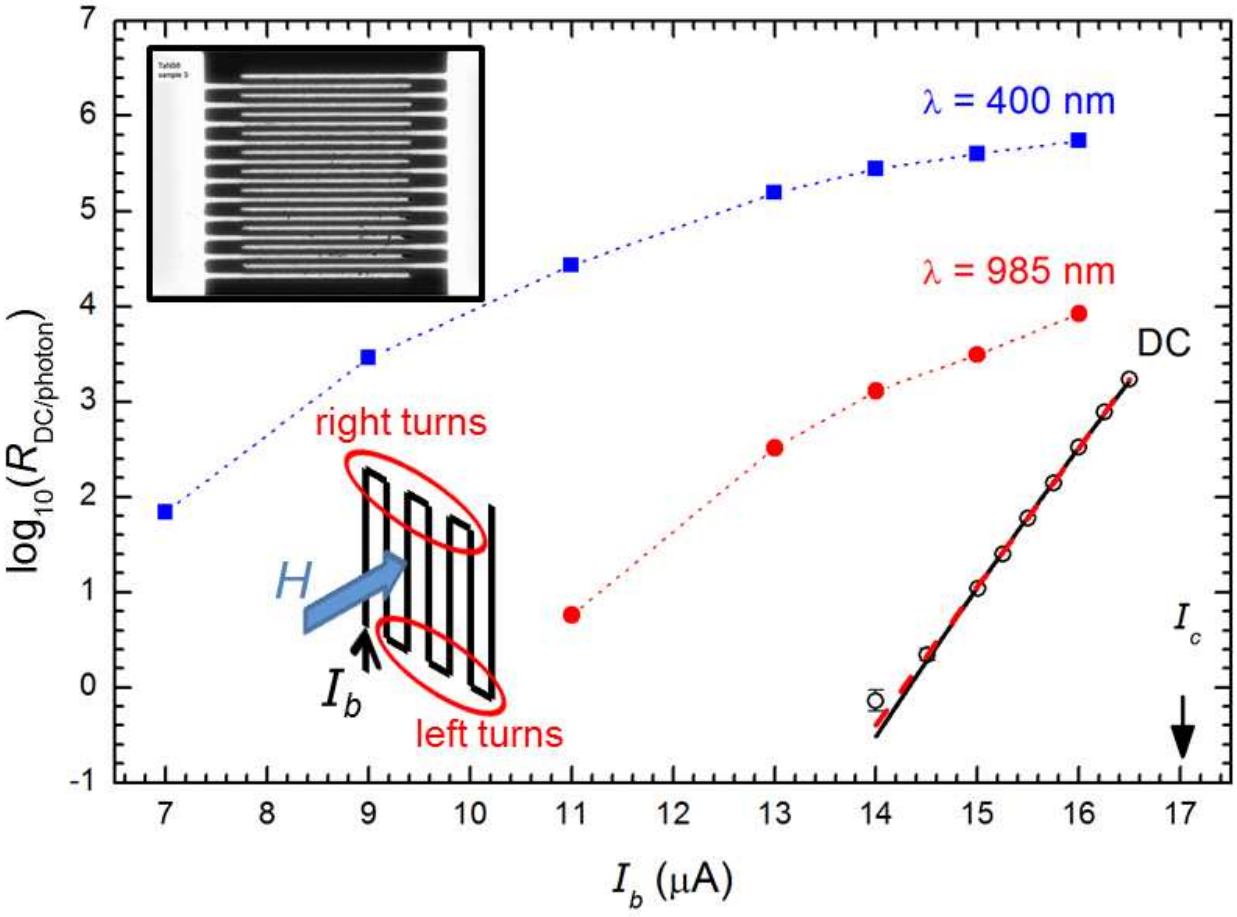

FIG. 1: Dark counts and photon counts on logarithmic scale *vs.* bias current. Errors are of the size of the data points or smaller except where plotted. The solid line is a least-squares fit to Eq. (51) from Ref. 6, while the dashed line is a fit to the phenomenological Eq. (1). The dashed lines connecting the photon-counts data are guides to the eye. The inset shows an electron micrograph of the measured device. In the lower left corner is a sketch of the magnetic field and bias current in relation to the meander geometry.

to -10 mT.

Following a recent theoretical model for vortex-crossings in straight strips[8] we would expect a symmetric field-dependence of the dark-count rate around $H = 0$, $R_{\rm DC}(H) \propto \cosh(H/H_1)$, with H_1 being a magnetic-field scale for vortex crossings. This behavior is clearly not compatible with the measured data, even if taking into account that the meander geometry consists of several parallel straight strips with alternating current directions. The self-field of one strip amounts to at most about 150 μT at the edges and the contributions

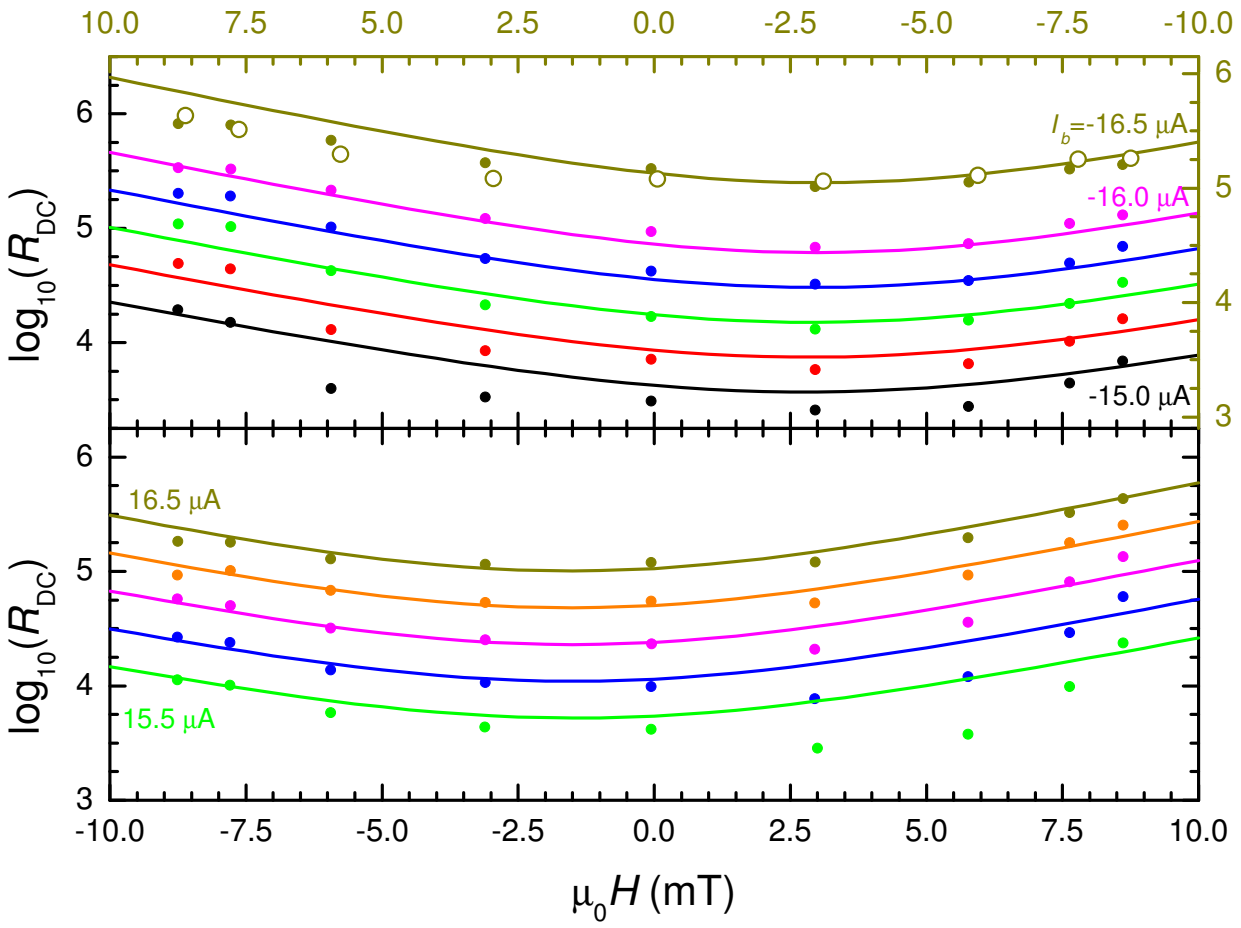

FIG. 2: Dark counts $\log(R_{\rm DC})$ for different I_b plotted as a function of applied magnetic field H. The $|I_b|$ have been progressively increased by 0.25 μA. Upper panel: $I_b < 0$; lower panel: $I_b > 0$. The +16.5 μA data are also plotted in the upper panel, but on a reversed field-axis (uppermost H-axis) to demonstrate the equivalence of reversing field or current direction. The corresponding y-axis (right axis, upper panel) has been shifted by 0.35 to compensate the current off-set. Solid lines are least-square fits according to Eq. (4) with common parameters, performed independently for negative and positive I_b, respectively.

from all the neighboring strips partly cancel each other, resulting in a maximum contribution of $\approx \pm 20$ μT, which is too small to explain the observed asymmetry in $R_{\rm DC}(H)$.

A more plausible explanation is that the 180° turnarounds connecting neighboring strips are responsible for the asymmetry in the magnetic-field dependence, which we will demonstrate in the following.

In general, a single 180° turnaround is expected to have a reduced critical current $I_{c,t}$

as compared to the straight strip ($I_{c,s}$)[17]. Applying the equations for the sharp rectangular 180° turnaround to our geometry, we calculate a reduction $\alpha = I_{c,t}/I_{c,s} \approx 0.5$. Estimating the critical current of the straight sections $I_{c,s} = 2wI_0/(\pi e\xi)$, with $I_0 = \Phi_0\mu^2/(2\mu_0\Lambda)$ at 4 K, and using the T-dependence of Λ and ξ and $\xi(0) \approx 5$ nm from $H_{c2}(T)$ measurements[11], we have $\alpha \approx 17\ \mu$A/22.6 μA ≈ 0.75. The measured α is larger than the theoretical value, most probably because our turnarounds are not strictly rectangular, but somewhat rounded.

Furthermore, it becomes clear that for bias currents $I_b \lesssim I_{c,t}$, the barriers for vortex-entry along the straight sections of the meander are still relatively high. Using Eq. (1) and scaling $\tilde{I}$ with I_c we estimate the probability for vortex-crossings near the turnaround to be a factor $\sim 10^5$ higher than along the straight sections, making vortex-crossings near the turnarounds the dominating contribution to R_{DC} despite their short overall length.

The application of a magnetic field destroys the symmetry of the current distribution in left- and right-turning turnarounds. In one case (e.g. left turn) screening currents due to the applied field will increase the current density at the inner edge (lower experimental I_c), while in the other case (right turn) it will decrease the current density (higher I_c). For magnetic fields $H \ll H^*$, with H^* being a device-dependent field scale for the critical current, the critical current is linear in magnetic field[8,17],

$$I_c(H) \approx I_{c,t}\left(1 - \frac{H}{H^*}\right),\ H^* = \frac{2w}{\pi e\xi}H_0,\ H_0 = \frac{\Phi_0}{2\mu_0 w^2}, \tag{2}$$

with $I_{c,t}$ the critical current in zero-field, and we obtain $\mu_0 H^* \approx 425$ mT for our device.

In Ref. 8, the magnetic-field dependence of the dark-count rate was obtained by replacing I_b with the true microscopic current at the edge which is the sum of applied current and screening current. We will take here a complementary approach by identifying the critical current for which the barrier for vortex entry vanishes with the field-dependent critical current from Eq. (2)[17]. Inserting Eq. (2) into (1) results in the field-dependent dark-count rate for a single 180° turnaround

$$R^1_{\mathrm{DC}}(H) = R_0 \exp\left(\frac{I_b}{\tilde{I}(1 - H/H^*)}\right). \tag{3}$$

The application of a positive magnetic field would then lead to a reduction of the critical current and thus an increased dark-count rate, whereas a negative field leads to a reduction of $R^1_{\mathrm{DC}}(H)$. Considering the geometry of our meander (see Fig. 1), we have an equal number of left- and right-turns with opposite effects of positive and negative applied fields on I_c,

and the overall effect of a magnetic-field should again be symmetric around $H = 0$. In reality, however, we may not expect that all of the turns are identical due to imperfections from the structuring process, and we have to assume a certain distribution of α-factors. In order to keep the model as simple as possible, we assume one turn to have a reduced critical-current (by a factor $\beta \leq 1$) and all others to have equal $I_{c,t}$. We then arrive at the following equation for the field-dependent dark-count rate, neglecting the contributions from the straight sections with $I_{c,s} > I_{c,t}$,

$$R^M_{\mathrm{DC}}(H) = (N-1)R^1_{\mathrm{DC}}(H) + R^\beta_{\mathrm{DC}}(H) + NR^1_{\mathrm{DC}}(-H), \tag{4}$$

with $R^\beta_{\mathrm{DC}}(H) = R_0 \exp\left[I_b/\left(\beta\tilde{I}(1-H/H^*)\right)\right]$ and $N = 10$ the number of left and right turns, respectively for the measured device. We performed independent least-squares fits to our data obtained for positive and negative currents (solid lines in Fig. 2), with $\mu_0 H^* \approx$ 240 mT, $\beta = 0.94 \pm 0.01$ and $\tilde{I} = 0.35 \pm 0.01$ μA as additional fitting parameters to the attempt rate R_0. $\tilde{I}$ compares well with $\tilde{I} = 0.31 \pm 0.01$ μA from fits of Eq. (1) to the zero-field $R_{\mathrm{DC}}(I_b)$ data. The field-scale H^* is smaller than the expected value calculated with Eq. (2) possibly due to edge imperfections generally leading to reduced edge barriers. However, our simple, vortex-based model obviously fairly accurately describes both the magnitude of and the observed asymmetry in the measured $R_{\mathrm{DC}}(H)$ with reasonable physical parameters.

In Fig. 3 we present our measurements of photon count-rates R_{ph} as functions of the applied magnetic field, normalized to the photon count-rates in zero-field and for two photon wavelengths of 400 nm and 985 nm, respectively. Dark-counts (typically $\ll 0.1R_{\mathrm{ph}}$, compare Fig. 1) have been subtracted. The estimated detection efficiencies (DE) range from ~ 0.1 at maximum I_b and 400 nm photons, to $\approx 10^{-4}$ at the lowest measured I_b and 985 nm photons. From the DE up to 0.1 we can conclude that most photon-detection events occur along the straight sections of the meander[18], which is also supported by recent simulations[23]. Except for the scattering in some datasets, R_{ph} appear to be constant with a *field-independent* photon count-rate.

Next, we will estimate the expected field-dependence following Ref. 8 for the photon count-rate at 985 nm wavelength, R_{985}, and $I_b = 13$ μA, for which the field-dependence should be most pronounced. Assuming that for 400 nm photons and $I_b = 16$ μA we have reached the maximum DE $\approx R_{\mathrm{abs}}$, the photon-absorption rate, we obtain for the photon-assisted vortex-crossing rate $\frac{R_{985}(13\ \mu\mathrm{A})}{R_{\mathrm{abs}}} = 1 - \exp(-2\eta) = 6 \cdot 10^{-4} \approx \eta$ (Eq. (45) in [8])[26].

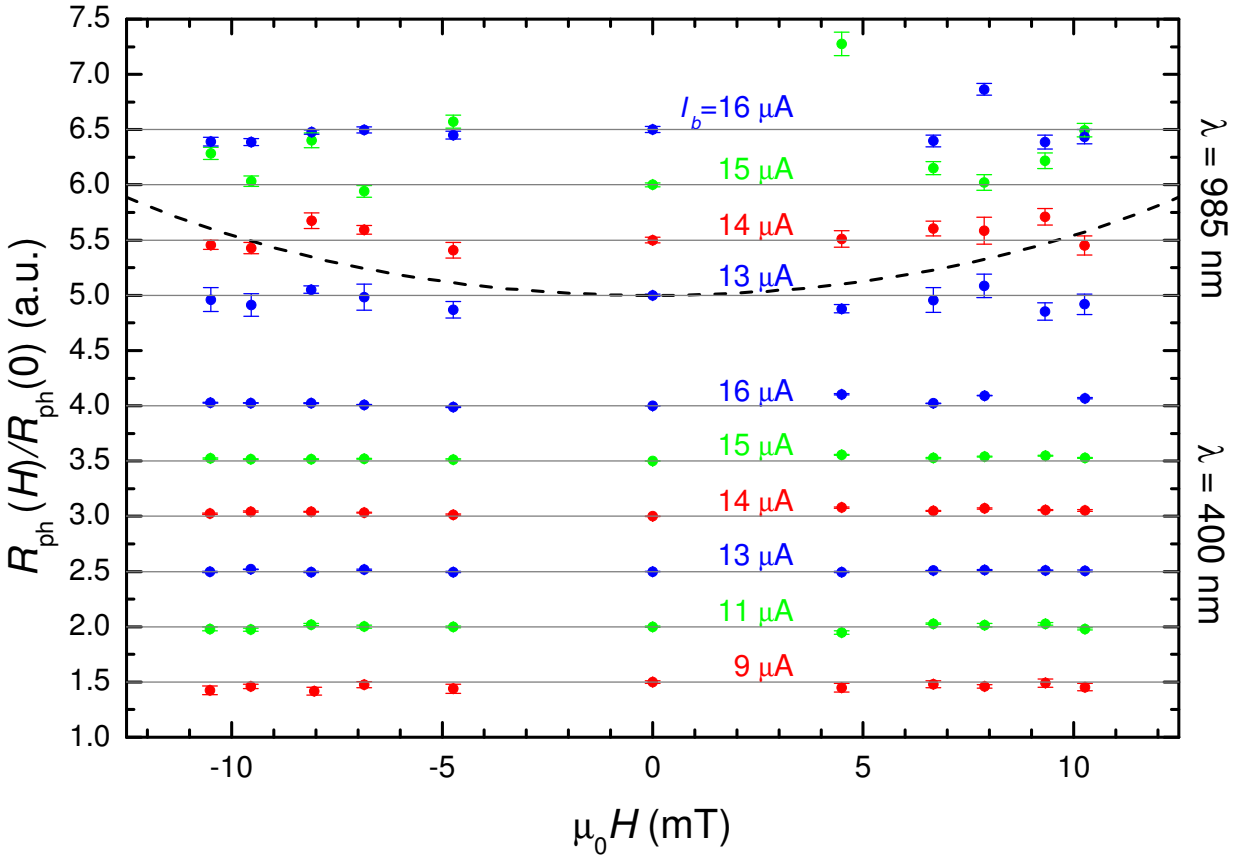

FIG. 3: Relative photon count-rates as functions of the applied magnetic field H, normalized to photon count-rates in zero-field for each I_b. For clarity, the datasets have been shifted in y-direction by multiples of 0.5. We also plotted the expected H-dependence for 985 nm photons and $I_b = 13$ μA (dashed black curve). Horizontal lines are to guide the eye.

With $\eta \ll 1$ Eq. (47) in [8] can be simplified to

$$\frac{R_{985}(H)}{R_{985}(0)} \approx \cosh\left(\frac{H}{H_{1h}}\right), \tag{5}$$

with $H_{1h} = H^* (\nu_h + 1)^{-1} I_b/I_{c,s}$, and ν_h is the vortex energy-scale near the absorption site that can be estimated from the low-current part in Fig. 1, where $R_{\rm ph} \propto I^{\nu_h}$, see Eq. (46) in [8]. We estimate $\nu_h \approx 12$ and therefore, using the larger, theoretical H^*, we obtain $\mu_0 H_{1h} \approx 10$ mT at $I_b = 13$ μA. The expected field-dependence is plotted in Fig. 3 (dashed curve) and would be easily measurable, which is clearly inconsistent with our data, however. A similarly strong field dependence would be expected for 400 nm photons and $I_b = 9$ μA ($\mu_0 H_{1h} \approx 12.5$ mT), whereas H_{1h} for the other datasets is expected to be larger and the field-dependence less pronounced, yet should still be measurable.

We note here that we have obtained qualitatively similar results also in NbN-SNSPD[8],[27], which shows that our observations are not unique to the TaN material.

In conclusion, we have presented systematic measurements of dark-count rates and photon-count rates as a function magnetic field in a TaN-SNSPD. The field-dependence of $R_{\mathrm{DC}}(H)$ can be successfully modeled assuming vortices traversing the superconducting strip predominantly in the vicinity of the meander turns, where the critical current for vortex-entry is reduced with respect to the straight sections. The observed asymmetry in R_{DC} with respect to current- or field-reversal can be explained assuming that not all turnarounds have exactly the same $I_{c,t}$. By contrast, we have not found any evidence for a scenario in which vortices assist in the detection of photons with energies that are insufficient to trigger a detection event. Our results strongly suggest that although crossing vortices are the main source of dark-counts, they most probably do not contribute significantly to the photon detection.

We acknowledge stimulating discussions with L. Bulaevskii and A. Semenov. This research received support from the Swiss National Science Foundation grant No. 200021_135504/1 and is supported in part by DFG Center for Functional Nanostructures under sub-project A4.3.

---

* andreas.engel@physik.uzh.ch

[1] J. R. Clem, in *Bull. Am. Phys. Soc.* (1998), vol. 43, p. 411.

[2] G. M. Maksimova, Phys. Solid State **40**, 1607 (1998).

[3] G. Stan, S. B. Field, and J. M. Martinis, Phys. Rev. Lett. **92**, 097003 (2004).

[4] F. Tafuri, J. R. Kirtley, D. Born, D. Stornaiuolo, P. G. Medaglia, P. Orgiani, G. Balestrino, and V. G. Kogan, Europhys. Lett. **73**, 948 (2006).

[5] C. Qiu and T. Qian, Phys. Rev. B **77**, 174517 (2008).

[6] L. N. Bulaevskii, M. J. Graf, C. D. Batista, and V. G. Kogan, Phys. Rev. B **83**, 144526 (2011).

[7] D. Y. Vodolazov, Phys. Rev. B **85**, 174507 (2012).

[8] L. N. Bulaevskii, M. J. Graf, and V. G. Kogan, Phys. Rev. B **85**, 014505 (2012).

[9] A. Gurevich and V. M. Vinokur, Phys. Rev. B **86**, 026501 (2012); L. N. Bulaevskii, M. J. Graf, and V. G. Kogan, *ibid.* **86**, 026502 (2012).

[10] G. N. Gol'tsman, O. Okunev, G. Chulkova, A. Lipatov, A. Semenov, K. Smirnov, B. Voronov, A. Dzardanov, C. Williams, and R. Sobolewski, Appl. Phys. Lett. **79**, 705 (2001).

[11] H. Bartolf, A. Engel, A. Schilling, K. Il'in, M. Siegel, H.-W. Hübers, and A. Semenov, Phys. Rev. B **81**, 024502 (2010).

[12] M. Hofherr, R. D., K. Ilin, M. Siegel, A. Semenov, H.-W. Hübers, and N. A. Gippius, J. Appl. Phys. **108**, (pages 9) (2010).

[13] J. R. Clem and K. K. Berggren, Phys. Rev. B **84**, 174510 (2011).

[14] H. L. Hortensius, E. F. C. Driessen, T. M. Klapwijk, K. K. Berggren, and J. R. Clem, Appl. Phys. Lett. **100**, 182602 (2012).

[15] D. Henrich, P. Reichensperger, M. Hofherr, K. Il'in, M. Siegel, A. Semenov, A. Zotova, and D. Y. Vodolazov (2012), arxiv:1204.0616.

[16] M. K. Akhlaghi, H. Atikian, A. Eftekharian, M. Loncar, and A. H. Majedi (2012), arXiv:1205.4290.

[17] J. R. Clem, Y. Mawatari, G. R. Berdiyorov, and F. M. Peeters, Phys. Rev. B **85**, 144511 (2012).

[18] K. Il'in, M. Hofherr, D. Rall, M. Siegel, A. Semenov, A. Engel, K. Inderbitzin, A. Aeschbacher, and A. Schilling, J. Low Temp. Phys. **167**, 809 (2012).

[19] A. Engel, A. Aeschbacher, K. Inderbitzin, A. Schilling, K. Il'in, M. Hofherr, M. Siegel, A. Semenov, and H.-W. Hübers, Appl. Phys. Lett. **100**, 062601 (2012).

[20] W. J. Skocpol and M. Tinkham, Rep. Prog. Phys. **38**, 1049 (1975).

[21] N. R. Werthamer, E. Helfand, and P. C. Hohenberg, Phys. Rev. **147**, 295 (1966).

[22] P. H. Kes and C. C. Tsuei, Phys. Rev. B **28**, 5126 (1983).

[23] G. R. Berdiyorov, M. V. Milošević, and F. M. Peeters, Appl. Phys. Lett. **100**, 262603 (2012).

[24] See Supplemental Material at [URL will be inserted by publisher] for details on how we determined T_c and other material and device parameters.

[25] Using a dipolar approximation for the field, the relative variations over the detector area are $< 10^{-7}$ and the in-plane component is estimated $< 1\%$, even for moderate misalignments.

[26] A factor of 2 is missing in Eq. (45) in [8], since vortices and anti-vortices contribute to the count-rate.

[27] See Supplemental Material at [URL will be inserted by publisher] for NbN data.

Supplemental Material: Magnetic-field dependence of count rates in superconducting thin-film TaN single-photon detectors

A. Engel, A. Schilling, K. Il'in, and M. Siegel

I. EARLIER RESULTS OBTAINED WITH A NBN SNSPD

At the early stages of our investigations, NbN SNSPD had been installed to check for a possible magnetic-field dependence of count rates. These first data sets are not as comprehensive as those taken later for the TaN SNSPD, which we present in the main text, but the general observed trends and conclusions for NbN are the same as for TaN. In Fig. 1 we show the magnetic-field dependence of dark-count rates (lower panel) and photon-count rates with 1000 nm wavelength (upper panel), measured with a NbN SNSPD (see Tab. I below for device parameters) at $T = 4$ K. The dark-counts show a qualitatively similar field-dependence as those measured with the TaN detector, with a clear asymmetry in the data with respect to the direction of H. Fitting Eq. (4) from the main text, we obtain a satisfactory description of the data (red line in the lower panel of Fig. 1) with the following fitting parameters: $\tilde{I} = 1.0 \pm 0.2$ μA and $\mu_0 H^* = 330 \pm 75$ mT. Here, there are $N = 12$ left and right turns, and the critical-current reduction factor $\beta = 0.9$ was held fixed.

The photon-count rates, on the other hand, *do not show any sign of field-dependence.* At a wavelength of 1000 nm, the detection efficiency has dropped by about two orders of magnitude as compared to the detection efficiency in the "plateau region". Following the same method as for the TaN detector to determine the field-dependence as expected from Ref. [8], we estimate the relevant field-scale $\mu_0 H_{1h} \approx 12$ mT. The resulting hypothetical field-dependent photon count-rate is plotted as the red-line in the upper panel of Fig. 1. It is obvious from that figure that the measured field dependence is much smaller than anticipated in Ref. [8].

II. MATERIAL PARAMETERS OF DETECTORS

In Tab. I we summarize relevant material and device parameters of the TaN and NbN SNSPD. The number of strips n_s is given by the meander design, and the film thickness

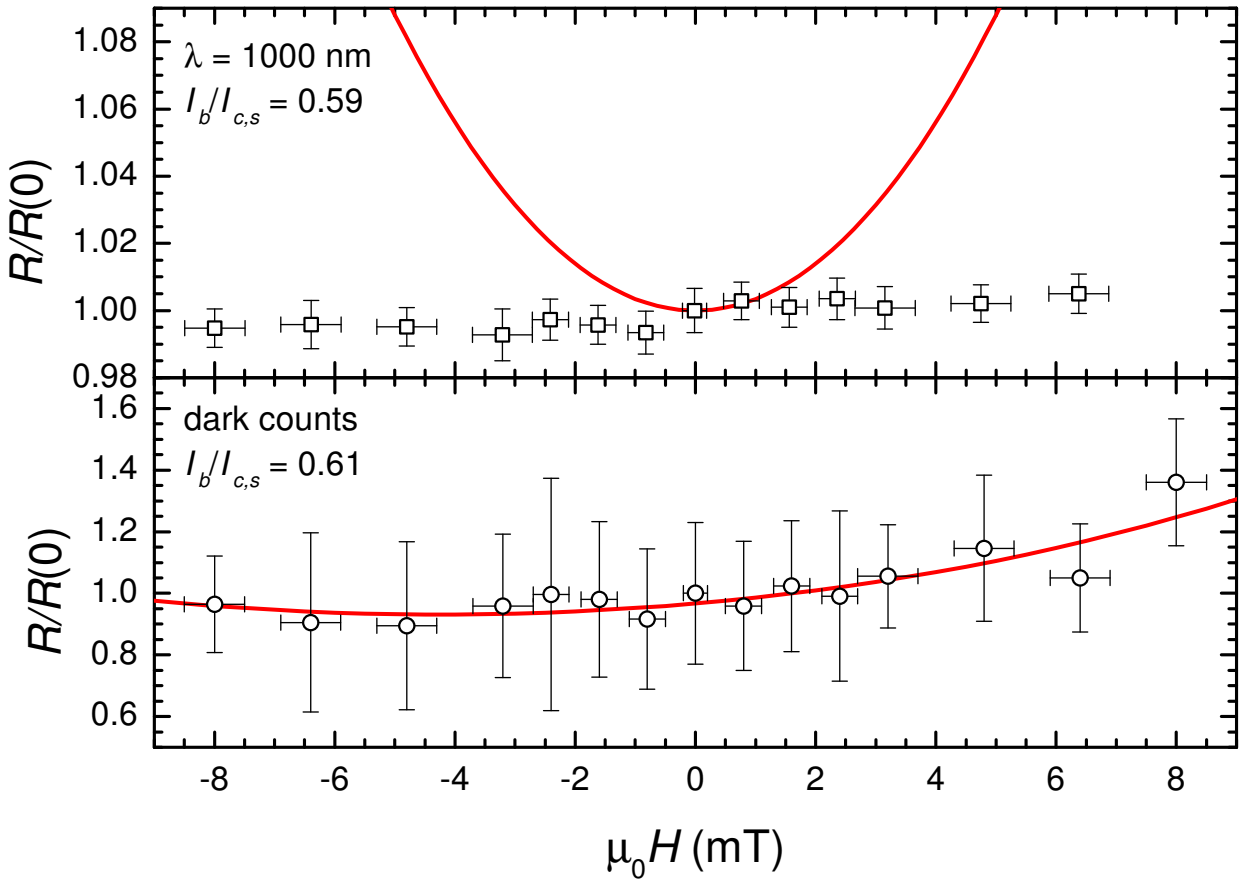

FIG. 1: Relative dark counts (lower panel) and photon count-rates (upper panel) as a function of magnetic field measured with a NbN SNSPD at $T = 4$ K. The red line in the lower panel is a least-square fit of Eq. (4) of the main text to the data, and the red line in the upper panel is the expected field-dependence of photon count-rates according to Ref. **?** . The error-bars on the x-axis stem from a preliminary-only magnetic-field calibration at the time of the measurements.

is inferred from the deposition time and previously determined deposition-rates. The strip widths were measured from scanning electron microscope images, for the TaN SNSPD from the actually measured device and for the NbN SNSPD from another device with the same design parameters.

Resistance R vs. temperature T measurements were done in a *Quantum Design Physical Property Measurement System*. The critical temperature T_c and the normal-state resistivity ρ_N in zero-field were determined applying fluctuation-conductivity theory for two-dimensional systems[20] to the resistance data above T_c, similar to Ref. [11]. The upper critical field $H_{c2}(T)$ was determined from resistance data in magnetic fields up to $\mu_0 H = 9$ T

TABLE I: Material and device parameters of the TaN and NbN SNSPD. Details are described in the text.

	n_s	d (nm)	w (nm)	ρ_N ($\mu\Omega$m)	T_c (K)	ξ (nm)	λ (nm)	$I_{c,e}$(4 K) (μA)	$I_{c,s}$(4 K) (μA)
TaN	21	4.9	110	2.2	8.84	5.2	520	17.0	22.6
NbN	25	6.0	80	2.3	13.1	4.1	400	32.3	52.5

applying a 50%-criterion. Extrapolating $H_{c2}(T)$ to $T = 0$ K and applying the correction of Werthamer[21], we obtained the zero-temperature coherence length ξ. The zero-temperature penetration depth λ was estimated using an approximation for dirty type-II superconductors[22], $\lambda = 1.05 \times 10^{-3}(\rho_N/T_c)^{0.5}$ in SI-units.

The experimental critical current $I_{c,e}$ was defined as the maximum current before the transition to the normal-conducting state in IV-characteristics, measured with applied voltage bias. These measurements were done in our optical ^{3}He-cryostat, with either the exit shutter of the monochromator closed, or blanks instead of the optical windows installed. The largest recorded critical current from over 20 measurements at a given temperature T was taken as $I_{c,e}(T)$. The temperature-dependent theoretical current of vanishing vortex-barriers for the straight strip $I_{c,s}(T)$ was calculated from the respective zero-temperature formula[8] and using approximate relations for the whole temperature-range[11]: $\xi(T) = \xi(1-t)^{0.5}(1+t)^{0.25}$ and $\lambda(T) = \lambda(1-t^2)^{0.5}(1+t^{1.5})^{0.25}$, $t = T/T_c$.

References

[8] L. N. Bulaevskii, M. J. Graf, and V. G. Kogan, Phys. Rev. B **85**, 014505 (2012).

[11] H. Bartolf, A. Engel, A. Schilling, K. Il'in, M. Siegel, H.-W. Hübers, and A. Semenov, Phys. Rev. B **81**, 024502 (2010).

[20] W. J. Skocpol and M. Tinkham, Rep. Prog. Phys. **38**, 1049 (1975).

[21] N. R. Werthamer, E. Helfand, and P. C. Hohenberg, Phys. Rev. **147**, 295 (1966).

[22] P. H. Kes and C. C. Tsuei, Phys. Rev. B **28**, 5126 (1983).